RSC Advances

PAPER

View Article Online
View Journal | View Issue

Cite this: *RSC Adv.*, 2024, **14**, 2862

Fluorinated polyether-coated Fe_3O_4-functionalized oxidized carbon nanotubes as a recyclable demulsifier for crude oil emulsion treatment

Chao Liu,[a] Lixin Wei,*[a] Weining Qin,[a] Yuxin Gu[a] and Xinlei Jia[ab]

Based on the excellent adsorption properties of carbon materials, a new magnetic nanodemulsifier was prepared in this study. First, carbon nanotubes were oxidized using a solvothermal method. Then, Fe_3O_4 was combined with oxidized carbon nanotubes using a one-pot method, and then grafted onto fluorine-containing polyether to prepare a magnetic composite demulsifier (Fe_3O_4@C–F) with good demulsification properties. The surface morphology of the composite demulsifier was analyzed using scanning electron microscopy (SEM). The structure of the composite demulsifier was characterized using Fourier transform infrared (FTIR) spectroscopy and X-ray photoelectron spectrometry (XPS). The stability of the composite demulsifier was characterized using thermogravimetric analysis (TGA). Results showed that the oxidized carbon nanotubes and fluorinated polyether were successfully attached to Fe_3O_4. The experimental objective was to obtain a self-made crude oil emulsion. The demulsification test and recovery performance test were then performed, and the main factors affecting the demulsification performance of the demulsifier were investigated. Results showed that when the dosage was 800 mg L^{-1}, the temperature was 65 °C, the demulsification time was 90 min, and the pH value was 6. The demulsification effect of the Fe_3O_4@C–F magnetic composite demulsifier was the best, whereby the demulsification rate could reach 91.68%, and the oil–water interface was clear. Fe_3O_4@C–F had a magnetic response and could be recycled from the two-phase system six times under the action of an external magnetic field. Fe_3O_4@C–F is an efficient and environmentally friendly demulsifier that has important application value for enriching demulsification technology systems.

Received 6th October 2023
Accepted 27th December 2023

DOI: 10.1039/d3ra06796c

rsc.li/rsc-advances

1. Introduction

The demand for oil is increasing day by day. Owing to the continuous development of oil fields, crude oil and water are getting mixed. In the process of tertiary oil recovery and heavy oil development, a large number of natural surfactants enter the process and can form a stable emulsion under the action of temperature, shear stress, and extrusion.[1,2] These stable emulsions can cause serious corrosion or obstruction to equipment and pipelines.[3–5] The improper treatment of oily wastewater can cause serious harm to the ecological environment and human health.[6,7] Therefore, there is a need to develop new environmentally friendly and efficient demulsifiers.

Polyether demulsifiers, renowned for their non-ionic characteristics, have been extensively investigated and applied as demulsification agents. Their exceptional design versatility has empowered researchers to tailor distinct polyether demulsifiers to suit the specific characteristics of diverse crude oil compositions. In the block composition, a segment with lipophilicity is usually polymerized, and then a segment with hydrophilicity is connected. When the polymerization is completed, the demulsifier molecule has enhanced surface activity.[8,9] Fluorinated surfactants are the most active surfactant found at present and have high thermal stability, hydrophobicity and oleophobicity. Moreover, they have good wetting and flocculation abilities,[10] which can effectively act on the oil–water interface to achieve the purpose of demulsification and dehydration. Based on these advantages, our team successfully introduced fluorine into polyether demulsifiers in the early stage, and then synthesized fluorine-containing polyether demulsifiers with fluorine-containing phenol as the starting agent, in addition to ethylene oxide (EO) and propylene oxide (PO).[11–13] Although fluoropolyether demulsifiers can promote the demulsification effect, they can cause pollution and are not easy to recycle. In response to green and sustainable concepts, magnetic demulsifiers have been developed. Magnetic nanoparticles have received considerable attention owing to their rapid response to

[a]*College of Petroleum Engineering, Northeast Petroleum University, Daqing 163318, China. E-mail: weilixin73@163.com*

[b]*Department of Chemical Engineering and Safety, Binzhou University, Binzhou 256603, China*

external magnetic fields and their recyclability. Among them, Fe_3O_4 nanoparticles are considered to be an ideal magnetic material due to their low cytotoxicity and good biocompatibility.[14] At present, most of the reported magnetic demulsifiers are composed of a magnetic Fe_3O_4 core and modified functional shell.[15,16] Zhao *et al.*[17] successfully synthesized polyethyleneimine (PEI)-coated Fe_3O_4 magnetic nanoparticles by a one-step solvothermal method. With increase in dosage, the demulsification efficiency was improved. Moreover, the recovery experiments showed that PEI-coated Fe_3O_4 could be reused up to ten times, thus showing good reusability. Yan *et al.*[18] synthesized a magnetic nanodemulsifier Fe_3O_4@PEI@β-CD with high interfacial activity using polyethyleneimine (PEI), β-cyclodextrin (β-CD), and Fe_3O_4. Results showed that under acidic, neutral and alkaline conditions, when the dosage of Fe_3O_4@PEI@β-CD was 200 mg L^{-1}, the temperature was 45 °C, and the sedimentation time was 30 min, the demulsification rate was greater than 95%. In the recyclability test, after recycling for 11 times, the demulsification efficiency did not considerably decrease and had a good demulsification effect. Fang *et al.*[19] used polypropylene oxide–polyethylene oxide and acetylacetone iron as raw materials to prepare a PEMN demulsifier by a one-step method. PEMN was endowed with magnetism, and the demulsification experiment showed that when the amount of demulsifier was 0.625 g L^{-1}, PEMN had an obvious demulsification ability after precipitation at 70 °C for 30 min. PEMN could be recycled, and the demulsification effect was good after three cycles. However, owing to the coating of crude oil in the magnetized demulsifier system prepared in this work, the difficulty of recovery increased and the number of cycles decreased. Therefore, in future research, the content of the surface functional compounds could be appropriately reduced to increase the saturation magnetic field strength of the magnetized demulsifier such that the magnetized demulsifier could respond well to the external magnetic field while having a better demulsification ability. In addition, Hamed *et al.*[20] recently prepared Fe_3O_4 nanomagnetic compounds based on imidazole-modified cyclodextrin (Fe_3O_4@β-CD@IL). For (30 : 70 vol%) W/O emulsion, the demulsification rate of Fe_3O_4@β-CD@IL could reach 92%, and the demulsifier could be reused for five times, which proved the potential of the magnetic compounds under different ionic liquids. TeAl-Janabi *et al.*[21] grafted graphene oxide nanosheets with polyethylene glycol-*block*-polypropylene glycol-*block*-polyethylene glycol triblock copolymer functionalized Fe_3O_4@SiO_2 to synthesize an amphiphilic magnetic nanodemulsifier (MND). The MND could quickly demulsify W/O emulsions and could be reused for at least four cycles. The spider-like structure, nano-size, amphiphilicity, and magnetic high density and high specific surface area of MND synergistically promoted the dispersion of MND and promoted rapid demulsification. Moreover, Fe_3O_4 can be re-grafted with other molecules, directly grafted with organic molecules, and compounded with inorganic particles. The Fe_3O_4 system is thus more diverse. However, the surface groups of pure Fe_3O_4 magnetic particles are not rich enough, the chemical properties are unstable, and it is easy to oxidize; thus, it is difficult to be directly applied. Therefore, it is often modified using various surface modification techniques.[22] Among them, carbon nanotubes have a unique hollow structure, ultra-high specific surface area, and good chemical stability.[23,24] In many studies, functional groups are added to the surface of carbon nanotubes to improve the adsorption selectivity of carbon nanotubes. However, carbon nanotubes have certain problems such as a difficulty in separation. The preparation of magnetic carbon nanotubes by compounding with magnetic nanoparticles can effectively compensate for the problems of Fe_3O_4 and carbon nanotubes.

In this study, based on the previous evidence that fluorinated polyether demulsifiers show a significant demulsification effect in crude oil emulsions, we developed a functional magnetic demulsifier with environmental sustainability and easy recovery.

First, the carbon nanotubes were modified, and then new composite demulsifiers of Fe_3O_4, oxidized carbon nanotubes and fluoropolyether were synthesized using a one-pot method. The synthesized composite demulsifier was characterized, and the factors affecting the demulsification effect and recovery rate were investigated. The Fe_3O_4@C–F demulsifier displayed a magnetic response, and could be recovered and reused from the two-phase system under the assistance of a magnetic field, which helped improve the demulsification efficiency of the emulsion and realize the recovery and reuse of the demulsifier. It has important application value for enriching demulsification technology systems.

2. Materials and methods

2.1. Materials

Iron acetylacetonate (≥98%) was purchased from Shanghai Yien Chemical Technology Co., Ltd. Oleic acid (≥85%) and anhydrous ethanol (≥99%) were purchased from Tianjin Tianli Chemical Reagent Co., Ltd. Oleylamine (70%) and dibenzyl ether (≥95%) were purchased from Shanghai McLean Biochemical Co., Ltd. Concentrated sulfuric acid (98%) and concentrated nitric acid (70%) were purchased from Sinopharm Group Chemical Reagent Co., Ltd. Multi-walled carbon nanotubes were purchased from Shenzhen Hongda Chang Evolution Technology Co., Ltd., and *n*-hexane (99%) was purchased from Tianjin Kaitong Chemical Reagent Co., Ltd. The purity of the abovementioned reagents was of analytical grade. Fluorinated polyether was prepared through previous experiments in the laboratory.[25] The dehydrated crude oil was supplied by an oil field of China National Petroleum Corporation (the density at 25 °C was 0.96 g mL^{-1}, the viscosity at 50 °C was 743.8 mPa s, and the total water content was 0.5%).

2.2. Methods

2.2.1. Preparation of Fe_3O_4@C–F. First, oxidized carbon nanotubes were prepared by a mixed acid oxidation method. Here, 0.5 g CNTs was dispersed in a mixed solution of 150 mL HNO_3 (70%) and 50 mL H_2SO_4 (98%), stirred, and ultrasonically treated for 1 h to uniformly disperse the CNTs in the mixed acid solution. Then, the black suspension was placed in a water

bath, heated to 80 °C, refluxed for 10 h, and cooled to room temperature. Distilled water was slowly added, until the suspension was diluted to 2 L, and it was then centrifuged at a rate of 8000 rpm for 10 min to obtain a black solid. The solution was then repeatedly washed with deionized water and centrifuged until the pH of the washing water was about 7. After vacuum drying at 80 °C for 24 h, a uniform black powder product, namely, oxidized carbon nanotubes (OX-CNTs), was obtained.

Next, Fe_3O_4@C–F was prepared by a one-step method, in which 0.001 mol iron acetylacetonate, 0.003 mol oleic acid, 0.003 mol oleylamine, 5 g fluorine-containing polyether, and 0.1 g OX-CNTs were added to a beaker, and 30 mL dibenzyl ether was added. Then, the material in the beaker was evenly stirred and ultrasonically dispersed for 30 min. The reagents in the beaker were then poured into the reactor, and the air in the reactor was removed by nitrogen. The reactor was placed in a muffle furnace at 230 °C for 5 h. After the heat preservation experiment, the reactor was taken out and placed in the air for natural cooling. After the reaction, the product in the kettle was taken out, and the magnetic demulsifier product was separated by a magnet, and a 1 : 1 volume mixture of ethanol and *n*-hexane was added to the product to clean the magnetic demulsifier product for 3–5 times. Finally, the product was dried at 60 °C for 12 h (Fig. 1).

2.2.2. Preparation of the water-in-crude oil emulsion. The crude oil emulsion was prepared from a mixture of 50% dehydrated crude oil and 50% NaCl solution (1.0 wt%). The mixture was heated at 60 °C for 30 min in a constant temperature water bath. Preheated crude oil was then added to a precision force-increasing electric stirrer, followed by the gradual addition of NaCl solution. Each stirring cycle occurred at 2000 rpm for 30 min until the emulsion was fully stirred. The resulting crude oil emulsion was transferred into a clean beaker and left to stand at room temperature for 24 h without experiencing oil–water separation.

2.2.3. Demulsification performance test and recovery experiment operation. According to SY-T 5281-2000, the demulsification performance of Fe_3O_4, the composite of Fe_3O_4 and OX-CNTs (Fe_3O_4@C), composite of Fe_3O_4 and fluoropolyether (Fe_3O_4@F), and composite of Fe_3O_4, OX-CNTs, and fluoropolyether (Fe_3O_4@C–F) were evaluated by the bottle test method. First, the pre-prepared crude oil emulsion was separately packaged, and 10 mL emulsion was poured in to each test tube. Then, according to the experimental requirements, the synthesized magnetic nanoparticles were added to the pre-configured crude oil emulsion without adding the control group. The demulsifier was completely mixed with the crude oil emulsion by shaking the bottle with an electric stirrer for 5 min, and then placed in a 65 °C water bath to prevent the droplets from solidifying in the emulsion. Finally, the test tube was placed in a 65 °C water bath for static sedimentation, and the demulsification effect was observed after 5, 15, 30, 60, 90, and 120 min. The demulsification performance of synthetic demulsifiers is measured by recording the water separation volume of crude oil emulsions. The demulsification rate is calculated using the following formula:

$$\text{demulsification efficiency } (\%) = \frac{V_d}{V_0} \times 100\% \quad (1)$$

where V_d and V_0 are the volume of the water phase and the initial volume of water in each time period, respectively.

After the experiment, the demulsifier was separated from the oil–water two-phase solution with a magnet. Finally, the magnetic demulsifier was washed with a mixed solution of ethanol and *n*-hexane with a volume ratio of 1 : 1, and then cleaned by ultrasonic cleaning. The de-emulsifier was rinsed for

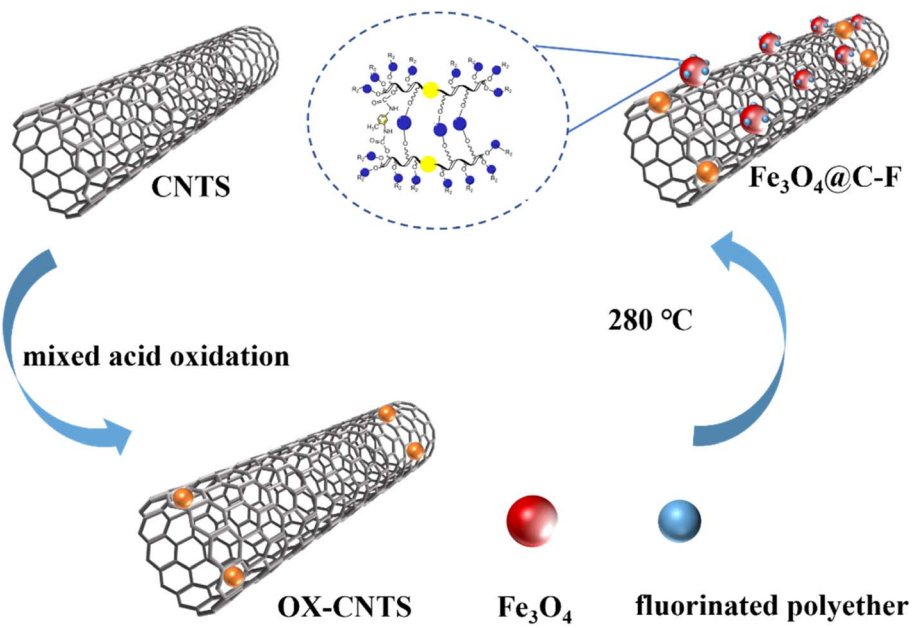

Fig. 1 Preparation of Fe_3O_4@C–F.

15 min, fully dispersed, and then recovered by an external magnetic field. The de-emulsifier was then rinsed three to four times until dissolution.

3. Results and discussion

3.1. Characterization of the Fe_3O_4@F demulsifier

3.1.1. Infrared spectroscopic analysis. Fig. 2 shows the infrared spectra of the oxidized carbon nanotubes, Fe_3O_4, and their composites. In the infrared spectrum of the oxidized carbon nanotubes, there was a characteristic peak of –OH functional group near 3389 cm^{-1}, which proved that the carbon nanotubes had been successfully oxidized. In addition, there were other active functional groups on the surface of the carbon nanotubes. The vibration absorption peak at 1719 cm^{-1} corresponded to the vibration peak of C=O, and the vibration absorption peak at 1641 cm^{-1} corresponded to the vibration peak of C=C. Comparing carbon nanotubes with Fe_3O_4@C, it was found that in addition to the functional groups of carbon nanotubes, Fe–O groups appeared at 552 cm^{-1},[26] indicating that Fe_3O_4 was successfully compounded with the carbon nanotubes. In addition, after the carbon nanotubes were attached to Fe_3O_4, the characteristic peak intensity of the active group was considerably weakened, indicating that the carbon nanotubes were stably attached to Fe_3O_4. In the FTIR spectrum of Fe_3O_4@F and Fe_3O_4@C–F, the stretching vibration absorption peaks of –CH and $-CH_2$ appeared at 2914 and 2825 cm^{-1}, respectively. The peak at 1242 cm^{-1} corresponded to the characteristic peak of C–O–C,[27] indicating the appearance of ether bonds. The stretching vibration peaks of F–C–F and C–F bonds existed at 1197 and 1206 cm^{-1}, indicating that the fluorinated polyether was successfully synthesized on the surface of Fe_3O_4@C and good chemical encapsulation was achieved.

3.1.2. Surface analysis and crystal structure. The surface elements of Fe_3O_4 and Fe_3O_4@C–F composites were characterized by XPS. The complete XPS spectrum was used to determine the introduction of oxidized carbon nanotubes and fluorine-containing materials on the surface of Fe_3O_4. Fig. 3(a) shows the complete XPS spectra of Fe_3O_4 and Fe_3O_4@C–F composites. It can be seen from Fig. 3(a) that all the main peaks of pure Fe_3O_4 specifically referred to Fe 2p, O 1s, and C 1s electrons, and the signals of Fe, O, and C elements appeared at about 723.1, 533.2, and 284.1 eV, respectively, which were the products of Fe_3O_4. For the Fe_3O_4@C–F composites, the strong peaks of C 1s and O 1s were detected by XPS, and the signal of F element was also observed at about 103.0 eV, indicating that the Fe_3O_4@C–F shell was formed and coated on the surface of Fe_3O_4. In addition, the high-resolution spectra of Fe_3O_4 and Fe_3O_4@C–F composites were also considerably different. Therefore, the surface structure of Fe_3O_4@C–F composites could be further determined by the high-resolution spectra obtained by XPS. The high-resolution XPS spectrum of the Fe_3O_4@C–F composite in the C 1s region is shown in Fig. 3(b). The C 1s spectrum of the Fe_3O_4@C–F composites could be divided into three peaks: C–O–C (287.8 eV), C=O (286.5 eV), and C=C (284.6 eV), with the C=C and C=O mainly from the oxidized carbon nanotubes and Fe_3O_4. Further, the presence of C–O–C linkages served as compelling evidence, confirming the successful incorporation of polyether moieties into the Fe_3O_4@O–CNTS composite. The O 1s peaks of Fe_3O_4@C–F composites were divided into three peaks at 529.9, 532.2, and 534.6 eV, corresponding to C=O, C–O, and C–OH bonds, respectively. According to the literature, the order of O 1s binding energy is OH > C–O > C=O. Therefore, the lower binding energy area of O 1s was attributed to the new bonds formed by O atoms between the surface functional groups of the oxidized carbon nanotubes and Fe_3O_4. The Fe 2p spectra of the Fe_3O_4@C–F composites are shown in Fig. 3(d). The two dominant peaks at 711.4 and 725.0 eV belong to Fe $2p_{3/2}$ and Fe $2p_{1/2}$ spin–orbit peaks.[28,29] Furthermore, the peaks at 712.4 and 727.0 eV were consistent with the Fe^{3+} ions of the Fe–O bond. The other two peaks at 711.2 and 723.9 eV were assigned to Fe^{2+} ions. In summary, these spectroscopic and crystallographic results confirmed the formation of the polyether-modified magnetic Fe_3O_4 nanoparticles.

3.1.3. Scanning electron microscopy. Fig. 4 shows the SEM images of the oxidized carbon nanotubes, Fe_3O_4, and their composites. The difference and change in the microstructure between the product and the raw material proved the formation of Fe_3O_4@C–F. From Fig. 4(a), it can be seen that carbon nanotubes had a typical tubular structure. Further, the columns were entangled with each other to form a network structure, and the arrangement of carbon nanotubes was relatively dense. In Fig. 4(b), it can be seen that Fe_3O_4 had a quasi-spherical shape, and its size distribution was almost uniform. Fig. 4(c) clearly shows that the Fe_3O_4@F composites were shaped like spherical flowers, and a large number of fluorine-containing polyethers were attached to the Fe_3O_4 nanoparticles. It can be seen from Fig. 4(d) that the oxidized carbon nanotubes were closely arranged and intertwined into irregular shapes, and that the smaller fluoropolyether molecules were closely attached to Fe_3O_4, and Fe_3O_4@F was loaded on the oxidized carbon nanotubes. This successful amalgamation of the three constituents ultimately yielded the desired Fe_3O_4@C–F composite.

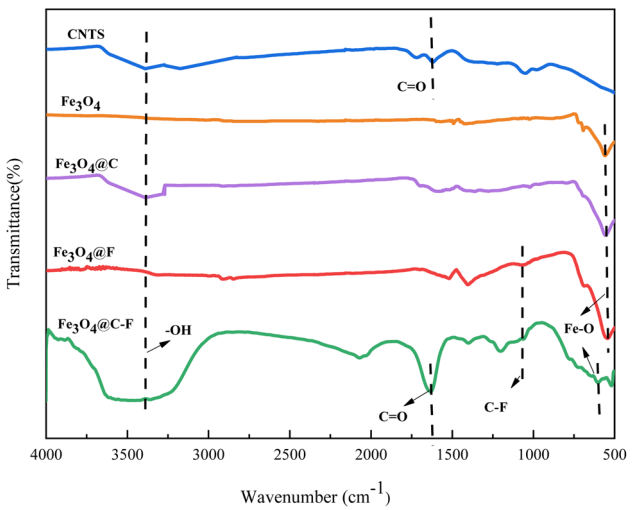

Fig. 2 Infrared spectra of the oxidized carbon nanotubes, Fe_3O_4, and their composites.

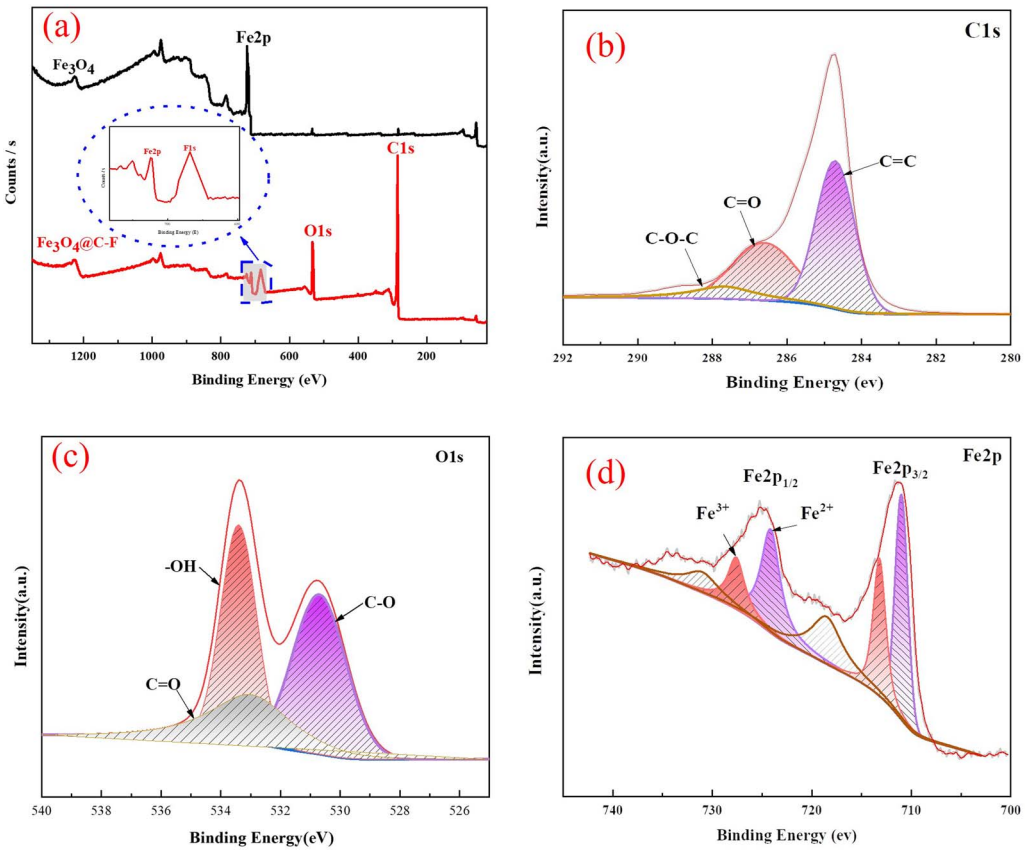

Fig. 3 Fe_3O_4@C–F demulsifier XPS full spectrum and Fe 2p, O 1s, C 1s spectra.

3.1.4. Thermogravimetry. Fig. 5 shows the TGA curves for the Fe_3O_4@F composites and Fe_3O_4@C–F composites with 0.05, 0.1, 0.15, and 0.2 g oxidized carbon nanotubes, respectively, which were obtained to study the thermal stability of the materials. At 37–90 °C, the weight of Fe_3O_4 composite nanomaterials suddenly decreased possibly owing to the removal of the associated water. When the temperature was between 90 and 350 °C, the weight of Fe_3O_4 composites decreased by about 5.5%, 8.6%, 5.8%, 4.9%, and 5.6%, respectively. This part of the weight loss was mainly attributed to the escape of the surface adsorbed gas and adsorbed water. In the temperature range of 350–550 °C, the weight of Fe_3O_4@F composites decreased by about 4.1%. Upon the introduction of O–CNTS, a marginal increase in the overall weight loss of Fe_3O_4@C–F composites was observed wherein the values recorded were 6.8%, 5.9%, 4.1%, and 5.4%. By comparing Fe_3O_4@F and Fe_3O_4@C–F, it could be seen that the thermal stability of Fe_3O_4@F was higher than that of Fe_3O_4@C–F. The main difference was the decomposition of the oxygen-containing functional groups on the surface of the Fe_3O_4@C–F oxidized carbon nanotubes. The higher weight loss observed in Fe_3O_4@C–F could be attributed to the elevated content of oxidized carbon nanotubes within the Fe_3O_4@C–F composite. The adsorbed water and adsorbed gas were responsible for the non-self weight loss of the composite material. When the non-self weight loss of the composite material was subtracted, the real weight loss of the composite material was about 5–6%. The total weight loss rates of Fe_3O_4@F and Fe_3O_4@C–F demulsifiers were lower, *i.e.*, less than 20%. The existence of C–F bonds in the Fe_3O_4 composite demulsifier will increase the decomposition temperature.

3.1.5. Wettability. The wettability characterization of the material can also indicate the performance of the material.[30] Fig. 6 shows the wettabilities of the Fe_3O_4, carbon nanotubes, oxidized carbon nanotubes, and Fe_3O_4@C–F by three-phase contact angle tests. The contact angles of Fe_3O_4 and O–CNTS were 21° and 52°, respectively, and the contact angle of CNTS was 109°. It could be seen that Fe_3O_4 and O–CNTS were hydrophilic, while CNTS was hydrophobic. After the oxidation reaction of carbon nanotubes, oxygen-containing groups, such as hydroxyl and carboxyl groups, were introduced, which changed the material from hydrophobic to hydrophilic. Studies have shown that when the contact angle of a material is 90°, the demulsifier has good demulsification performance. The contact angle of Fe_3O_4@C–F was 89°, close to 90°, which was consistent with the performance of the demulsification material. During the annealing process, some hydrophilic groups of Fe_3O_4@C–F were lost, which further improved the contact angle of the composite and the material demulsification performance.

3.1.6. Interfacial tension. The interfacial tension of an oil–water interface is a key factor affecting the demulsification effect. Fig. 7(a) shows the interfacial tension of Fe_3O_4@C, Fe_3O_4@F, and Fe_3O_4@C–F at 800 mg L^{-1}. All five materials

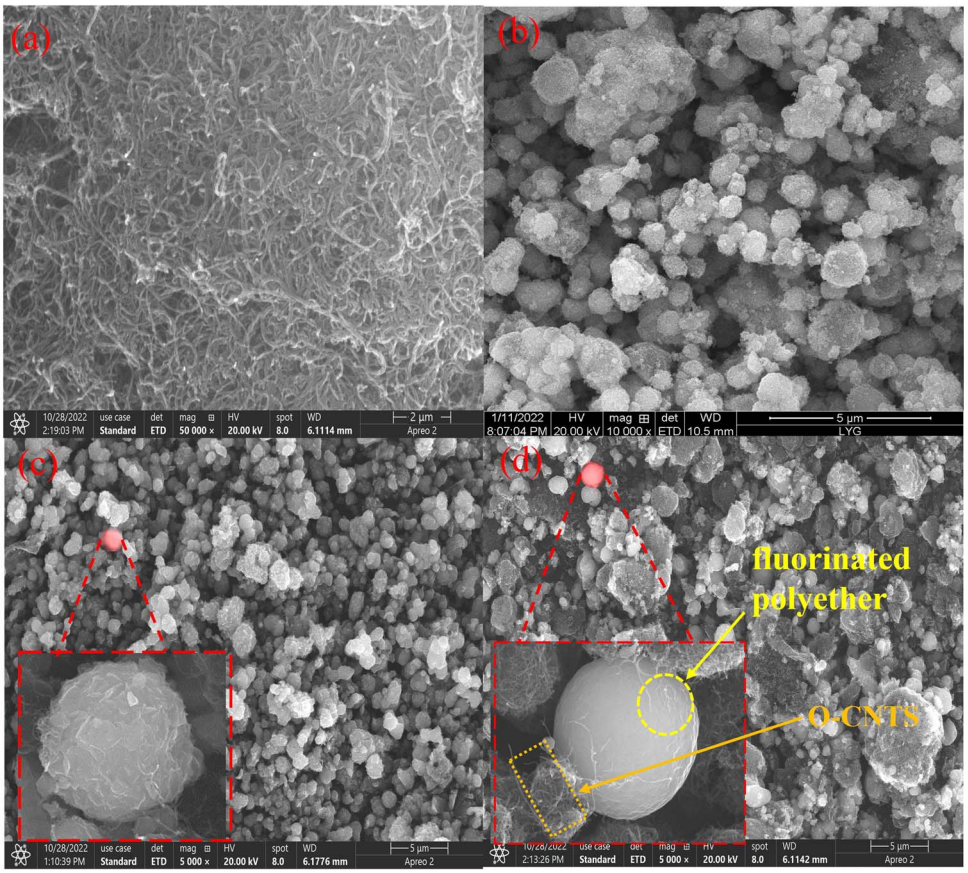

Fig. 4 SEM images of carbon nanotubes, Fe_3O_4, and their composites (a) O–CNTS, (b) Fe_3O_4, (c) Fe_3O_4@F, and (d) Fe_3O_4@C–F.

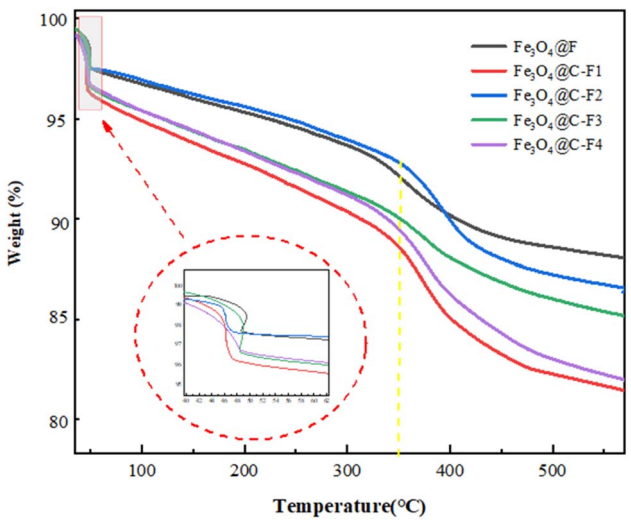

Fig. 5 Thermogravimetric analysis of the Fe_3O_4@F and Fe_3O_4@C–F composites with different contents of oxidized carbon nanotubes.

could considerably reduce the oil–water interfacial tension. Among them, Fe_3O_4@F had the strongest ability to reduce the interfacial tension, which could reduce the interfacial tension of the emulsion from 38.4 to 15.5 mN m^{-1}. The interfacial properties of the five materials were, in order from low to high, OX-CNTs, Fe_3O_4@C, fluorinated polyether, Fe_3O_4@C–F and Fe_3O_4@F. The interfacial properties of Fe_3O_4@C–F were better than those of OX-CNTs and fluorinated polyether monomers. Recently, many studies have suggested that the demulsification effect is determined by the interfacial activity and structure of the demulsifier. The interfacial tension of Fe_3O_4@C–F with different dosages is shown in Fig. 7(b). The interfacial tension decreased with the increase in demulsifier dosage, and the decrease range increased with the increase in demulsifier dosage. Results showed that for a demulsifier with the same structure, the higher the concentration, the lower the interfacial tension, and the better the demulsification effect of the demulsifier. In summary, the prepared Fe_3O_4@C–F composites had good interfacial properties.

3.2. Demulsification performance of the Fe_3O_4@C–F demulsifier

3.2.1. Effect of the demulsifier dosage on the demulsification effect. Fig. 8 shows the effect of different dosages of Fe_3O_4@C–F magnetic demulsifier on the demulsification effect when the experimental temperature was 65 °C. In the inset of Fig. 8, the test tubes shown in the diagram show the demulsification effects of the different dosages at 120 min. Fig. 8 shows that when the dosage of Fe_3O_4@C–F magnetic demulsifier was 800 mg L^{-1}, the demulsification effect was the best, whereas

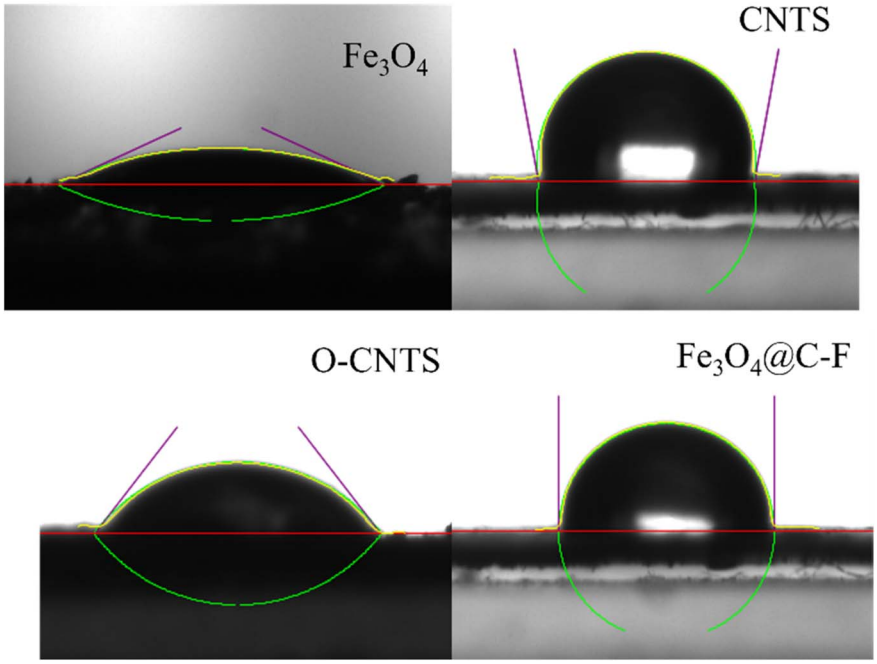

Fig. 6 Contact angles of Fe_3O_4, CNTS, O–CNTS, and Fe_3O_4@C–F.

when the dosage was 800 mg L^{-1}, it can be seen from the test tube in the inset that the solution was relatively clear and the oil droplet wall was less; it was also determined that the demulsification rate reached 91.39%. When the demulsifier dosage was less than 800 mg L^{-1}, the demulsification rate increased with the increase in demulsifier dosage. When the demulsifier dosage was 1000 mg L^{-1}, the demulsification ability became weaker.[31] For some magnetic materials, the coating material is lipophilic and Fe_3O_4 is hydrophilic. These magnetic materials can replace some natural surfactants to adsorb on the oil–water interface.[32,33] Here, Fe_3O_4@C–F has the same demulsification process. When the dosage was increased until the adsorption at the oil–water interface reached saturation, the interfacial stability of the emulsion was higher, and the demulsification efficiency decreased with the increase in dosage.

3.2.2. Effect of time and temperature on the demulsification. Four temperature gradients (35 °C, 50 °C, 65 °C, 80 °C) were set up to observe the demulsification effect of Fe_3O_4@C–F within 120 min under the dosage of 800 mg L^{-1} demulsifier. The results are shown in Fig. 9. With the increase in demulsification time and temperature, the demulsification efficiency increased. When the demulsification temperature was 80 °C and the action time was 120 min, the demulsification efficiency was the highest. However, when the temperature was in the

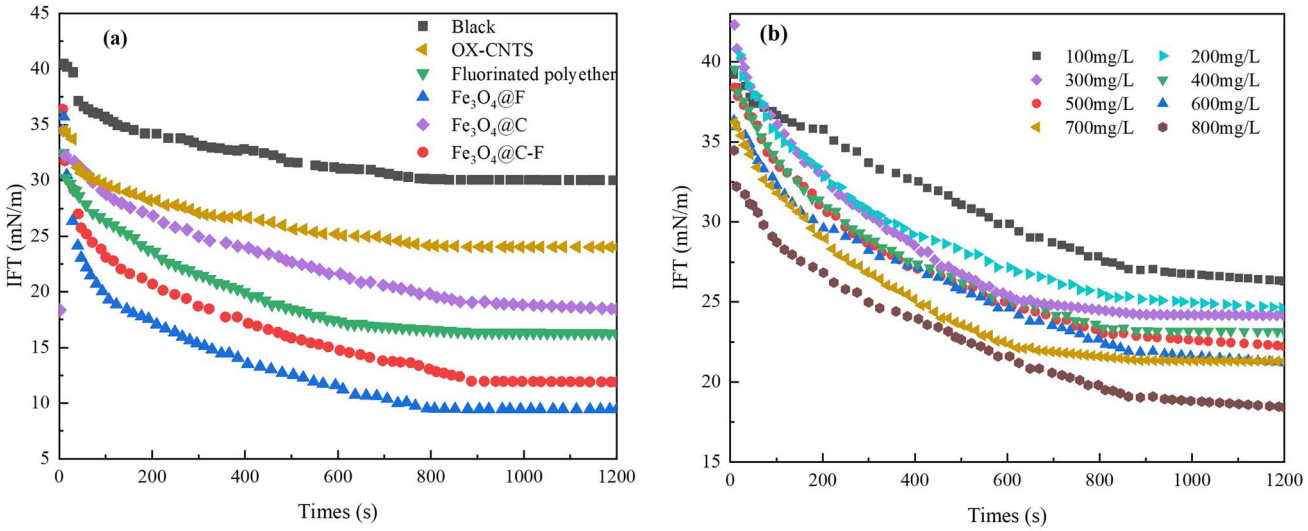

Fig. 7 (a) Interfacial tension of different materials. (b) Different amounts of interfacial tension.

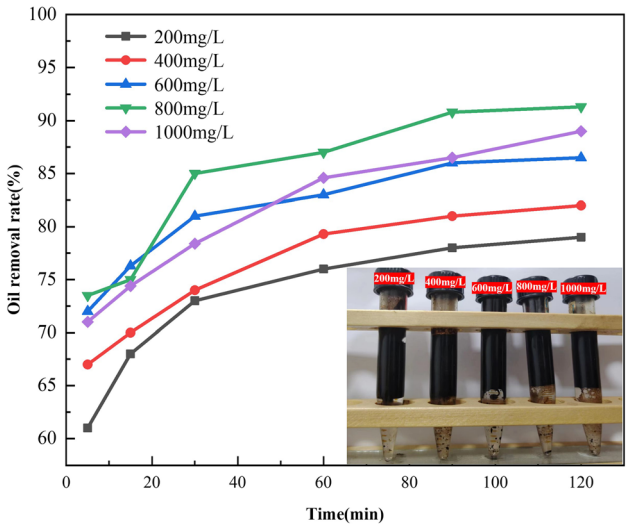

Fig. 8 Demulsification effect of Fe_3O_4@C–F under different dosages.

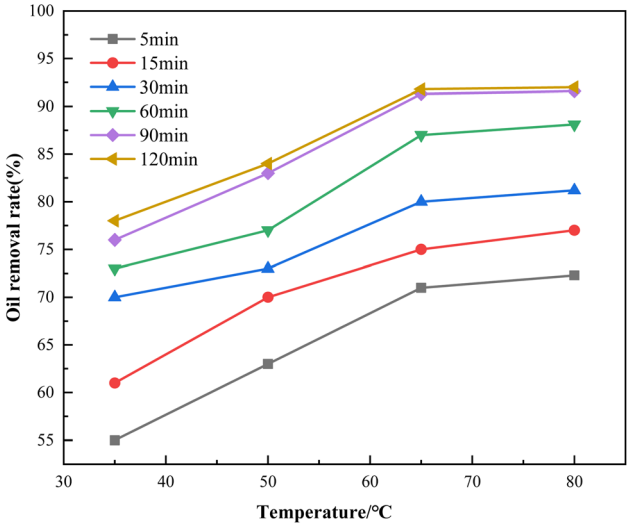

Fig. 9 Demulsification effect of the demulsifiers at different time changes with the temperature.

range of 50–65 °C, the demulsification efficiency of the magnetic demulsifier increased fastest in the different time periods, but when the temperature exceeded 65 °C, the demulsification rate was extremely slow. After adding the Fe_3O_4@C–F magnetic demulsifier, the demulsification efficiency of the crude oil emulsion exceeded 50% within 5 min, reflecting the high demulsification efficiency of Fe_3O_4@C–F. When the demulsification time reached 90 min, the demulsification effect of the crude oil emulsion was obvious, the demulsification rate reached 91.68%, and the adhesion of oil droplets decreased. When the precipitation time was extended to 120 min, the demulsification rate of the demulsifier increased by 2.6%, 1.2%, 3.4%, and 3.2%, under the four temperature gradients. It could be seen that the demulsification efficiency of demulsifier was improved, but the improvement was not obvious. Therefore, when the temperature reached 80 °C, even when the demulsification temperature was increased again, the increase in the demulsification efficiency of the demulsifier was extremely limited. Therefore, the optimum demulsification time for the Fe_3O_4@C–F magnetic demulsifier was set to 90 min and the temperature was set to 65 °C.

3.2.3. Effect of the pH value on the demulsification performance. Fig. 10(a) shows the effect of the Fe_3O_4@C–F magnetic demulsifier on the demulsification performance at different pH environments, with an experimental temperature of 65 °C and dosage of 800 mg L^{-1}. Under the optimal conditions, the demulsification rate of the Fe_3O_4@C–F magnetic demulsifier increased with the reduction in pH value. Therefore, the demulsification effect of magnetic nanoparticles was better at a low pH value. Among them, the demulsification rate was the highest at pH 6, and the demulsification performance was the best, and the highest demulsification rate could reach 91.3%. On this basis, the Fe_3O_4@C–F magnetic demulsifier with an experimental temperature of 65 °C and a dosage of 800 mg L^{-1} was selected to determine the zeta potential at pH 5, 6, 7, and 8. The results are shown in Fig. 10(b). With the increase in pH value, the zeta potential of Fe_3O_4@C–F gradually decreased, and the charge changed from positive to negative. At low pH values, H^+ was adsorbed on the surface of the Fe_3O_4@C–F magnetic particles, which made the surface positively charged and enhanced the electrostatic attraction between magnetic particles and negatively charged oil droplets, thus weakening the electrostatic repulsion between oil droplets and promoting the aggregation of oil droplets. At high pH values, the zeta potential of the Fe_3O_4@C–F magnetic particles was low, and the mechanical properties of the emulsion were relatively stable, and the demulsification rate decreased.

3.2.4. Recovery performance analysis. The magnetic saturations of Fe_3O_4, Fe_3O_4@C, Fe_3O_4@F, and Fe_3O_4@C–F were 47.4, 18.2, 38.5, and 35.2 emu g^{-1}, respectively. Compared with the saturation magnetization of Fe_3O_4, the magnetic strength of the Fe_3O_4 composites was considerably lesser, which was mainly caused by the magnetic field shielding effect of the polyether and carbon nanotubes. Moreover, by comparing the saturation magnetization of the three different Fe_3O_4 composite demulsifiers, it was found that the saturation magnetization of Fe_3O_4@CNTs was the lowest, which was mainly caused by the structural characteristics of the carbon nanotube materials. The oxidized carbon nanotubes were hollow tubular structures, and Fe_3O_4 was attached to the hollow tubular structure. Compared with polyether molecules, this shielding effect was stronger, resulting in a relatively low saturation magnetization of Fe_3O_4@CNTs. The magnetic saturation value of Fe_3O_4@F was the highest in the composites. This was because the fluorinated polyether molecules were relatively small and were more dispersed on the surface of Fe_3O_4, which indicated they had little effect on the magnetic response of the Fe_3O_4 particles. In addition, from Fig. 11(a), the hysteresis loops of Fe_3O_4 and its composite demulsifiers all passed the origin, which proves that the magnetic demulsifiers had no residual magnetization and coercivity; *i.e.*, the demulsifiers had superparamagnetism. Therefore, the Fe_3O_4 composite material can be effectively

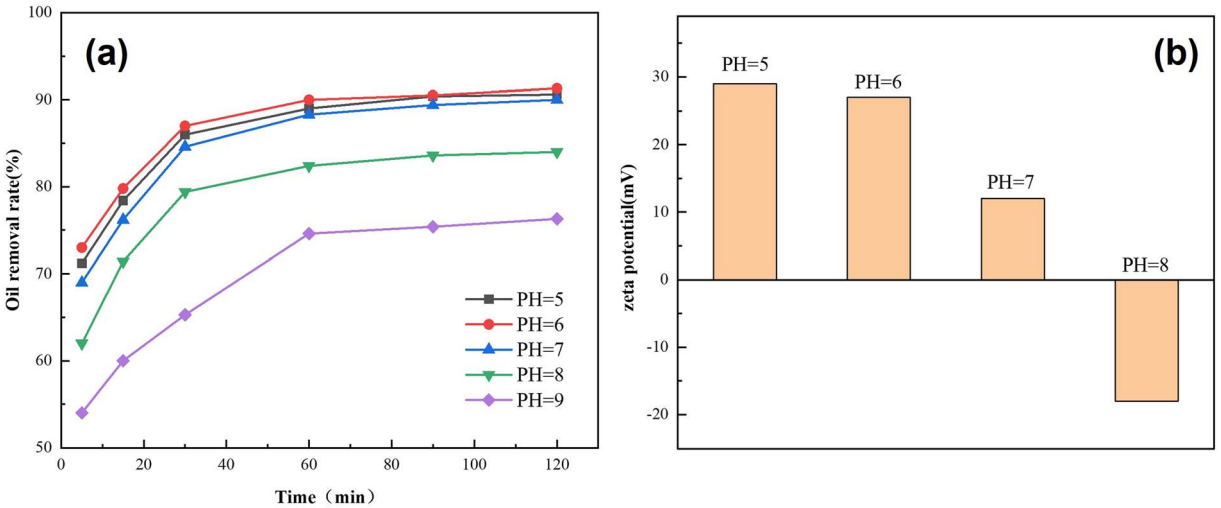

Fig. 10 Demulsification effect and zeta potential of the demulsifiers with different pH values.

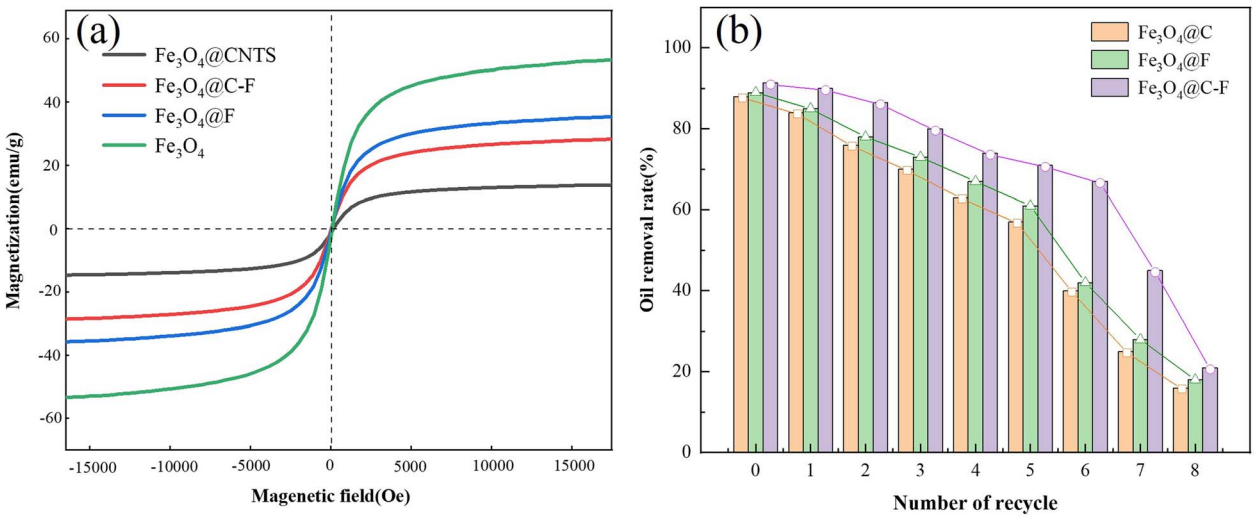

Fig. 11 VSM (a) and recovery tests (b) of Fe_3O_4 and its composites.

attracted by the external magnetic field such that it has the ability of magnetic recovery after demulsification. In the cycle test, the parameters were set as follows: temperature, 65 °C; demulsifier dosage, 800 mg L^{-1}; and reaction time, 90 min. The results are shown in Fig. 11(b). The demulsification efficiency of the Fe_3O_4 composites decreased with the increase in the number of cycles, but they showed excellent demulsification performance in the first six cycles, and the demulsification rate was above 60%. However, after seven times of recovery, the demulsification efficiency decreased sharply, and the demulsification efficiency was below 30% at the eighth time. The possible reason for this was that a certain amount of oil phase was adsorbed on the surface of the demulsifier, which could not be completely removed by washing, resulting in fewer adsorption sites of the magnetic demulsifier and affecting the performance of the demulsifier. As shown in Table 1, the recovery rate of Fe_3O_4@C–F decreased sharply after the sixth cycle; therefore, Fe_3O_4@C–F could not be recycled more than three or six times. This change may be due to the fact that the response of Fe_3O_4@C–F to the magnetic field became weaker after it was wrapped by crude oil during the demulsification process, which

Table 1 Recovery ratio of Fe_3O_4@C–F after each recycling test

Recycle no.	Recovery ratio of Fe_3O_4@C–F/%
1	97.12
2	94.23
3	88.9
4	87.4
5	75.4
6	65.3
7	22.4
8	10.8

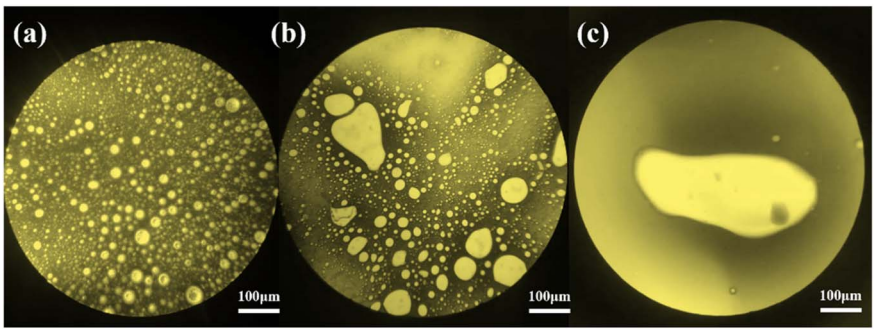

Fig. 12 Microscopic demulsification process of Fe_3O_4@C–F, (a) before demulsification, (b) during demulsification, (c) after demulsification.

hindered the recovery of Fe_3O_4@C–F. In summary, the Fe_3O_4 composite demulsifier not only has excellent demulsification performance but also has unique magnetic response performance. It performed well in the recovery experiment and displayed good recyclability. These characteristics could help it solve a series of environmental problems caused by the difficulty in separating traditional chemical demulsifiers after reaction.

3.2.5. Demulsification microscopic diagram and mechanism analysis. To explore the possible demulsification mechanism of Fe_3O_4@C–F, the crude oil emulsion was observed by optical microscopy, as can be seen in Fig. 12. In Fig. 12(a), the emulsion prepared in this study was a W/O type, where the dark color is oil, the light color is water, and the water phase is evenly distributed in the oil phase. After adding the demulsifier, it can be seen in Fig. 12(b) that the emulsion breaks, the water molecules aggregate, and large water droplets appear, forming a new interfacial film. After demulsification, it can be seen in Fig. 12(c) that the demulsification is gradually completed, and the oil and water are basically completely separated. In summary, the demulsification mechanism is proposed as follows. After adding the demulsifier, it absorbs and replaces the natural active agent contained in the emulsion, destroys the original rigid interfacial film, makes the emulsion structure unstable, and then oil–water separation occurs. The excellent demulsification effect of Fe_3O_4@C–F was mainly due to the synergistic demulsification effect of three parts: the fluorinated polyether plays a bridging role in promoting droplet aggregation; the surface of O–CNTS contains oxygen-containing active functional groups, such as hydroxyl groups, which enhance the adsorption capacity of droplets;[34] the Fe_3O_4 is positively charged under acidic and neutral conditions and can attract negatively charged droplets through electrostatic interaction. In addition, the different density between the separated oil and water phases is also helpful to achieve complete separation under the action of gravity.

4. Conclusions

In this study, a novel magnetic composite demulsifier was proposed. Fluorinated polyether and oxidized carbon nanotubes were combined on the surface of magnetic Fe_3O_4 nanoparticles by a one-pot method. Specifically, taking the crude oil of an oilfield as the experimental object, demulsification experiments were carried out on the magnetic demulsifier to study the main factors affecting the demulsification effect. The specific surface areas of the oxidized carbon nanotubes and Fe_3O_4 magnetic nanoparticles were large, and there were more points for adsorption on the surface of the material. Therefore, during the demulsification process, Fe_3O_4@C–F magnetic composites are more easily adsorbed at the oil–water interface, which improves the demulsification efficiency. When the dosage was 800 mg L^{-1}, the temperature was 65 °C, the demulsification time was 90 min, and the pH value was 6, the demulsification effect of the Fe_3O_4@C–F magnetic composite demulsifier was the best, and the demulsification rate could reach 91.68%. The magnetic composite demulsifier could be recovered by a magnet and reused six times while maintaining a high demulsification efficiency. The use of this recyclable magnetic composite emulsifier can reduce environmental pollution and operational complexity. The synthesis process is simple and is expected to promote the application of recyclable nanodemulsifiers in oil fields.

Conflicts of interest

The authors declare that they have no known competing financial interests or personal relationships that could have appeared to influence the work reported in this paper.

Acknowledgements

The authors are grateful for the reviewers' instructive suggestions and careful proofreading. This work was supported by the Natural Science Foundation Project of Heilongjiang Province (LH2022E025).

References

1 S. Park, E. S. Lee and W. R. W. Sulaiman, *J. Ind. Eng. Chem.*, 2015, **21**, 1239–1245.
2 A. Kamari, M. Sattari, A. H. Mohammadi and D. Ramjugernath, *Fuel*, 2015, **158**, 122–128.
3 I. Gavrielatos, O. Shoham, R. S. Mohan and R. Dabirian, *J. Fluids Eng.*, 2018, **141**, 021301.

4 A. A. Umar, I. B. M. Saaid, A. A. Sulaimon and R. B. M. Pilus, *J. Pet. Sci. Eng.*, 2018, **165**, 673–690.
5 P. K. Kilpatrick, *Energy Fuels*, 2012, **26**, 4017–4026.
6 L. Xia, S. Lu and G. Cao, *Chem. Eng. Commun.*, 2004, **191**, 1053–1063.
7 X. Wu, *Energy Fuels*, 2011, **17**, 179–190.
8 D. Ming, C. Wang, X. Song, S. Fang, Y. Ma and T. Tao, *Chem. Eng. J.*, 2016, **302**, 44–49.
9 R. Marquez, A. M. Forgiarini, D. Langevin and J. L. Salager, *Energy Fuels*, 2019, **33**, 8151–8164.
10 P. Riachy, G. Lopez, M. Emo, M. Stébé, J. Blin and A. Bruno, *J. Colloid Interface Sci.*, 2017, **487**, 310–319.
11 L. Wei, L. Zhang, S. Guo, X. Jia, Y. Zhang, C. Sun and X. Dai, *ACS Omega*, 2021, **6**, 25518–25528.
12 L. Zhang, L. Wei, L. Shi, X. Dai, S. Guo, X. Jia and C. Liu, *J. Polym. Res.*, 2022, **29**, 2–12.
13 X. Geng, C. Li, L. Zhang, H. Guo, C. Shan, X. Jia, L. Wei, Y. Cai and L. Han, *Molecules*, 2022, **27**, 1799.
14 J. Gong, B. Wang, G. Zeng, C. Yang, C. Niu, Q. Niu, W. Zhou and Y. Liang, *J. Hazard. Mater.*, 2009, **164**, 1517–1522.
15 T. Lü, Z. Shuang, D. Qi, Z. Dong and H. Zhao, *J. Colloid Interface Sci.*, 2018, **518**, 76–83.
16 M. Tanjim, M. A. Rahman, M. M. Rahman, H. Minami, S. M. Hoque, M. K. Sharafat, M. A. Gafur and H. Ahmad, *Soft Matter*, 2018, **14**, 5469.
17 H. Zhao, C. Zhang, D. Qi, T. Lü and D. Zhang, *J. Dispersion Sci. Technol.*, 2019, **40**, 231–238.
18 H. Yan, X. Yu, G. Dong, Z. Zhang, K. Ding, H. Yang and G. Su, *Colloids Surf., A*, 2023, **660**, 130877.
19 S. Fang, B. Chen, T. Chen, M. Duan, Y. Xiong and P. Shi, *Chem. Eng. J.*, 2017, **314**, 631–639.
20 S. Hamed, M. Zahra and A. Ebrahim, *Carbohydr. Polym.*, 2024, **327**, 121697.
21 O. Y. TeAl-Janabi, H. A. Abdulkareem, I. F. Waheed and P. J. S. Foot, *Colloids Surf., A*, 2023, **676**, 132228.
22 B. Zhang, R. Hu, D. Sun, T. Wu and Y. Li, *J. Chem. Eng. Data*, 2018, **63**, 4689–4702.
23 H. Wang, K. Lin, B. Jing, G. Krylova, G. E. Sigmon, P. McGinn, Y. Zhu and C. Na, *Water Res.*, 2013, **47**, 4198–4205.
24 Z. Huang, X. Luo, Y. Mi, G. Wu, C. Wang, L. Liu, F. Ye and Y. Luo, *Sep. Sci. Technol.*, 2020, **56**, 1–9.
25 L. Wei, M. Chao, X. Dai, X. Jia, X. Geng and H. Guo, *ACS Omega*, 2021, **6**, 10454–10461.
26 H. Qi, B. Yan and W. Lu, *J. Sol-Gel Sci. Technol.*, 2014, **69**, 67–71.
27 L. Zhang, L. Wei, L. Shi, X. Dai, S. Guo, X. Jia and C. Liu, *J. Polym. Res.*, 2022, **29**, 2–12.
28 D. Wilson and M. A. Langell, *Appl. Surf. Sci.*, 2014, **303**, 6–13.
29 K. Heba, F. Ahmed, E. Hesham and A. Adel, *Crystals*, 2021, **11**, 1153.
30 Y. Deng, C. Peng, M. Dai, D. Lin, I. Ali, S. S. Alhewairini, X. Zheng, G. Chen, J. Li and I. Naz, *J. Cleaner Prod.*, 2020, **266**, 121624.
31 W. Kang, G. Jing, H. Zhang, M. Li and Z. Wu, *Colloids Surf., A*, 2006, **272**, 27–31.
32 B. R. S. Lemos, A. P. C. Teixeira, J. D. Ardisson, W. A. A. Macedo, L. E. Fernandez-Outon, C. C. Amorim, F. C. C. Moura and R. M. Lago, *Appl. Sci.*, 2012, **2**, 513–524.
33 N. Ali, B. Zhang, H. Zhang, W. Zaman, X. Li, W. Li and Q. Zhang, *Colloids Surf., A*, 2015, **472**, 38–49.
34 H. Xu, W. Jia, S. Ren and J. Wang, *Carbon*, 2019, **145**, 229–239.